Optically Tuned Wide-Band Terahertz Modulation, Charge Carrier Dynamics and Photoconductivity of Femtosecond Laser Ablated Titanium Disulfide Nanosheet Devices

Qi Song, Lu Chai, Junqi Chen, Weining Liu, Qing Ma, Yanfeng Li, and Minglie Hu

***Abstract*—Based on femtosecond laser ablated processing, one-dimensional arrays with different line spacings were fabricated on titanium disulfide (TiS_2) nanosheet. Optical modulated measurements with these devices were demonstrated. Photo-induced complex conductivity changes of the TiS_2 nanosheet devices were studied by an optical-pump THz-probe (OPTP) measurement system. For the 700 μm line spacing device, the optically introduced modulation depth (MD) reached up to 70%. Our experimental results have demonstrated the ultrafast dynamics and photoconductivity for the TiS_2 nanosheet devices in the THz frequency range. TiS_2 nanosheet based devices would be suitable as the photoelectric modulators of THz wave.**

***Index Terms*—Terahertz modulator, nanomaterials, femtosecond pulse, ultrafast dynamics.**

I. Introduction

TITANIUM DISULFIDE (TiS_2), having an octahedral configuration with a Ti layer sandwiched between two S layers, is a typical 2D material with stability and excellent photoelectric properties, which has been previously developed for electrodes, photo-thermal therapy, saturable absorbers for lasers and photodetectors [1], [2]. The semimetallic TiS_2 can easily produce higher carrier concentration with mobility like that in a metallic band structure due to the apparent overlap of the valence and conduction bands [3], [4]. Therefore, TiS_2 shows great potential as optically introduced modulators in a rather wide wavelength range. Semiconductors have proven to be suitable for all-optical modulation of electromagnetic waves. The photo-excited free carriers could be produced by the incident photons with energy exceeding the band gap of the semiconductors, which is proportional to the flux of the incident photons [5]. Generally, optically-introduced modulation for terahertz (THz) radiation could be recognized as the following processes. When laser pulses are incident on the semiconductor, a temporary region of low transmittance to THz wave is produced. With the THz wave and laser beam co-incident onto this area, the THz transmittance will thus be modulated [6]. Optical modulators such as InSb, GaAs, ErAs/GaAs based devices have been reported [7]–[9]. Phase-transition VO_2 could also be used as optical modulators [10], [11]. However, the VO_2 based devices are easily damaged by laser power exceeding 120 mW [11]. With the development of material science, optically controlled active modulators based on graphene and graphene liked materials (for example, the transition metal disulfides-TMDs) such as SnS_2, WS_2, MoS_2 and WSe_2 have been reported from optical frequency to THz region[12]–[15]. These results have demonstrated that TMDs materials have larger absorption than graphene and therefore more suitable for optically-controlled active THz modulators [16], [17].

The previous studies on the optically-introduced THz modulators are based on TMDs with the band gap far above the THz wave energy [18]–[20]. And still few reports on near zero bandgap (near THz wave energy) TMDs fabricated devices for optical THz modulators. The TiS_2 material could absorb electromagnetic waves in the THz band by intraband transitions, while other TMDs such as WS_2, MoS_2 do not exhibit intraband transitions [21].

In this article, TiS_2 nanosheet-based devices with three line spacings have been ablated by a femtosecond laser. Then, the optical modulation by the devices were demonstrated experimentally. In addition, optical-pump THz-probe (OPTP) measurements were performed and photo-induced complex conductivity changes of the TiS_2 devices were demonstrated. Our results have shown the ultrafast dynamics and photoconductivity of TiS_2 nanosheet in the THz waveband and they would be suitable as the photoelectric modulators for the THz applications.

II. Fabrication and Characterization of the Disulfide Titanium Grating

The TiS_2 nanofilm could be prepared by the following steps. Firstly, put 0.3 g of TiS_2 powder with the dimensional of 100 μm

Manuscript received December 31, 2019; revised April 20, 2020 and May 3, 2020; accepted May 18, 2020. Date of publication May 22, 2021; date of current version June 17, 2020. This work was supported in part by the National Natural Science Foundation of China under Grants 61827821 and 61535009 and the Tianjin Research Program of Application Foundation and Advanced Technology under Grant 17JCJQJC43500. *(Corresponding author: Lu Chai.)*

The authors are with the Key Laboratory of Opto-electronic Information Technology (Ministry of Education), Ultrafast Laser Laboratory, School of Precision Instrument and Opto-electronics Engineering, Tianjin University, Tianjin 300072, China (e-mail: songqi1990@outlook.com; lu_chai@163.com; chenjunqi@tju.edu.cn; lwnlxh616@tju.edu.cn; 18822266535@163.com; yanfengli@tju.edu.cn; huminglie@tju.edu.cn).

Color versions of one or more of the figures in this article are available online at https://ieeexplore.ieee.org.

Digital Object Identifier 10.1109/JSTQE.2020.2996248

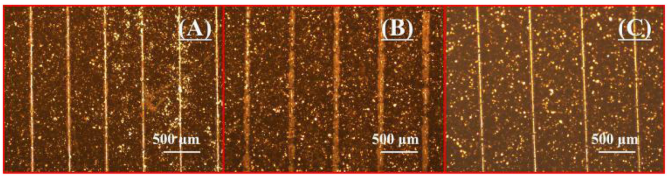

Fig. 1. Micrographs of TiS_2 devices with line spacings of (a) 500 μm, (b) 600 μm, and (c) 700 μm.

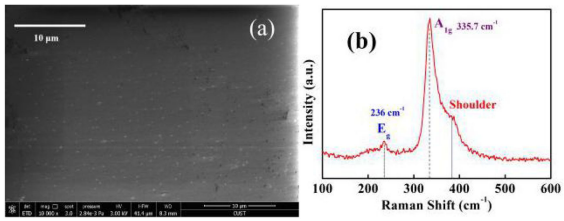

Fig. 2. (a) SEM photograph and (b) Raman spectra of TiS_2 nanosheet.

was put into 20 ml of mixture solution (alcohol mixed with water 3:1). Secondly, the mixed solution was stirred by ultrasound for 250 minutes. Then, the solution was centrifuged for one minute at the speed of 500 rpm. After that, the sub-layer liquid was collected and tiled on substrates with a 10 μm thickness spacer [22]. Finally, the substrates with the TiS_2 nanosheet were left at 25 °C overnight to thoroughly remove the liquid. And then the TiS_2 nanosheet-based substrates were ablated by a femtosecond laser [22]. This device could be mainly used in the fields of spectroscopy and filtering, etc. [23], [24].

The micrographs of the fabricated the TiS_2 devices with line spacing of 500 μm, 600 μm, and 700 μm are given in Fig. 1. The line width of these devices was about 20 μm. The sample size used in our experiment had a dimension of 20 mm $\times$ 20 mm. The SEM photograph and Raman spectrum of the TiS_2 nanosheet are shown in Fig. 2. In Fig. 2(a), the SEM photograph shows that the TiS_2 nanosheet with a size of 100 nm $\times$ 200 nm. In Fig. 2(b), the Raman spectra of the TiS_2 film show the 235 cm^{-1} and 335.7 cm^{-1} peaks related respectively to the E_g and A_{1g} vibrational modes and a shoulder at about 376 cm^{-1}. The shoulder peak at $\sim$376 cm^{-1} has been attributed to an interlayer vibrational mode, which could be due to excess interlayer metal atoms, causing in turn a stiffening of the phonon [25], [26]. The positions of the Raman peaks can confirm that the sample of TiS_2 is 1T phase and bulk feature [26], [27].

III. Experimental Setup

The experimental setup of OPTP system is shown in Fig. 3. Our measurements made use of optical excitation of the TiS_2 devices and probing of the THz response using time-domain spectroscopy.

The laser used for both optical pumping and THz probing was a home-made femtosecond Yb-doped photonic crystal fiber amplifier [28] (1040 nm center wavelength, 0.6 μJ pulse energy, 43 MHz repetition rate, 40 nm FWHM bandwidth, and 115 fs pulse duration). THz pulses were generated from the femtosecond laser pulses by optical rectification in a 3 mm GaP $<$ 110 $>$-cut crystal. The generated THz wave was collimated and

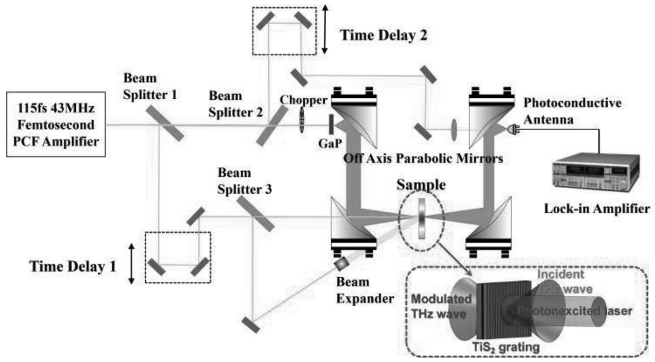

Fig. 3. Experimental setup of optical-pump THz-probe spectroscopy (OPTP) system.

focused by a pair of off-axis parabolic mirrors onto the sample. The size of the THz beam on the sample was about 3 mm. After passing through the sample, the diverging THz radiation was collimated and focused by another pair of off-axis parabolic mirrors onto a photoconductive antenna for the measurement of THz electric field. The sampling beam was scanned in the time domain by a mechanical translation stage. For optical excitation, the irradiated laser was incident onto the samples with a slightly tilted angle less than 5° from the surface. In order to homogeneously photo-excite the TiS_2 device, the pump beam diameter was expanded to 5 mm, larger than the spot size of the incident THz beam. Another mechanical translation stage was used in the pump beam path to vary the time delay between the THz probe pulse and the optical excitation pulse. All of the measurements were performed at room temperature.

IV. Results and Discuss

A. Measurements of the Optically Introduced THz Electric Field Modulation

The optically-induced THz modulation effect was measured by using a THz time-domain spectroscopy. We recorded the time-dependent electric field of the THz wave transmitted through the TiS_2 devices and nanosheet, defined as $E(t)$. As a reference, the THz electric field through a bare quartz substrate was defined as $E_0(t)$. Then, the corresponding (complex) frequency-domain fields, $E(\omega)$ and $E_0(\omega)$ could be obtained by the Fourier transform. Figs. 4 and 5 demonstrate the transmitted THz electric fields and the corresponding spectra, respectively, of the TiS_2 devices with 500, 600, 700 μm line spacings and the TiS_2 nanosheet modulated by different laser powers, respectively.

When TiS_2 was illuminated by femtosecond laser pulses, the THz modulation effect could be recognized clearly. As shown in Fig. 5, the electric field amplitude of the THz wave decreased continuously as the power of incident femtosecond laser gradually increased from 120 mW to 780 mW. When the pump power was increased to 250 mW, the average THz power decreased in the frequency range between 0.2 to 0.8 THz due to the increasing absorption coefficient [29]. Among the devices with the line spacing of 500, 600, and 700 μm, the maximum change in modulation amplitude appeared in the 700 μm line spacing device.

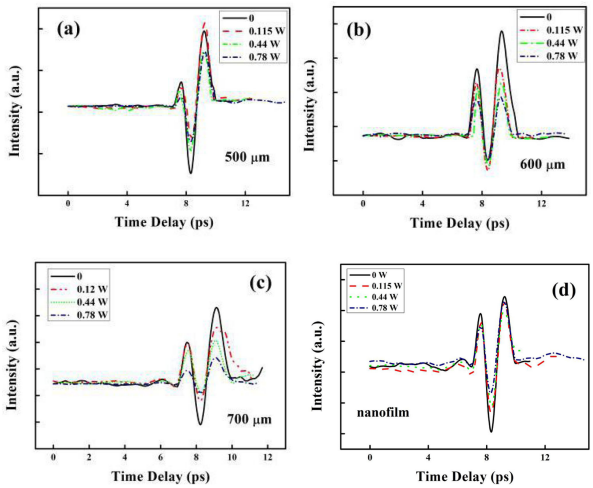

Fig. 4. Transmitted THz electric fields of TiS_2 devices with the line spacings (a) 500, (b) 600, (c) 700 μm, and of (d) TiS_2 nanofilm, modulated by different optical powers.

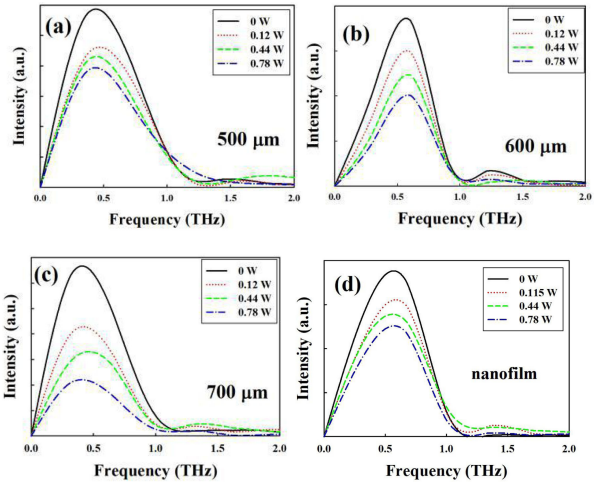

Fig. 5. The transmitted THz spectra corresponding to Fig. 4.

In order to evaluate the optically-introduced THz modulator, the modulation depth (MD) was defined as [30]:

$$\mathrm{MD} = \frac{|T_P - T_0|}{T_0} \tag{1}$$

where T_p and T_0 are the THz transmittances with and without laser incident on the modulators, respectively. The MD and the normalized THz transmittance for the devices with line spacings of 500, 600, 700 μm and the TiS_2 nanofilm without the lines as a function of the modulation beam power are shown in Fig. 6(a) and (b), respectively. From Fig. 6(a), it can be noted that the maximum MD of the 700 μm line spacing device can reach 70% at a pump laser power of 780 mW, while the MDs in the 30% to 50% range for the 500 and 600 μm line spacing devices and the TiS_2 nanosheet without the lines. The higher the pump laser, the larger the MD. These results suggest that the TiS_2 nanosheet-based structure could be employed as a wide-band modulator for the THz waveband.

The modulation property of the TiS_2 nanosheet without the lines can be attributed to its absorption of the THz wave, because

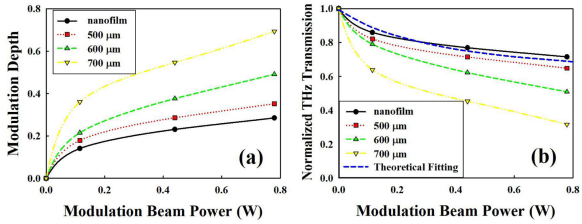

Fig. 6. MD (a) and normalized THz transmittance (b) for devices with line spacings of 500, 600, 700 μm and TiS_2 nanofilm as a function of the modulation beam power.

the photon energy of the THz wave is suitable for its band gap. Electron-hole carriers could be generated when the TiS_2 nanosheet was excited by a femtosecond laser at 1040 nm. Most carriers were then diffused rapidly until an equilibrium was reached. The nonlinear photo-response could be reinforced under a higher pump laser power, because a faster mobility in the TiS_2 nanosheet would enhance the MD [4].

For the devices of the TiS_2 nanosheet with the lines, the main appendant effect is in the frequency domain, due to the wire-grid-like structure. The MD of the devices is much higher than the TiS_2 nanosheet without the lines. Among of the samples, the transmitted frequencies become higher when through the 700 μm line spacing device with maximum MD, which is more suitable for the modulation by TiS_2.

In Fig. 6(b), the THz transmittance decreased with the increasing incident laser power for all samples. In general, the TiS_2 nanosheet would absorb and reflect more THz wave when the electric conductivity increases, resulting in a decrease in THz transmittance [14]. The optically-induced transmittance coefficient of the TiS_2 nanosheet could be written as [29], [31]:

$$T(E) = \frac{1}{\left(1 + \frac{1}{2}\alpha\pi\sigma\left(E\right)\right)^2} \tag{2}$$

where α is the fine structure constant. Ignoring the photon effect and other mechanical effects, the nonlinear conductivity caused by the strong laser could be expressed by Floquet expansion [16]:

$$\sigma\left(E\right) = \sqrt{\left(1 + \sigma_3\left(E\right)H_2\right)^2 + \sigma_3^2\left(E\right)H_1^2} \tag{3}$$

where, $\sigma_3(E) = \frac{e^2\nu_F^2E_0^2}{\hbar^2\omega^4}$, $H_1 = \frac{13}{48}N(\frac{1}{2}) - \frac{2}{3}N(1) + \frac{45}{48}N(\frac{3}{2})$, $H_2 = 2N(1)$, $N(x) = \tanh(\frac{x\hbar\omega}{2k_BT})$, e is the elementary charge, v_F is the Fermi velocity, E_0 is the strength of the incident field, ω is the frequency of the incident photons and T is the system temperature. The third- order conductivity of the TiS_2 nanosheet could be obtained by [30]:

$$\sigma_3(P) = \frac{e^2v_F^2}{\hbar^2\omega^4}\frac{2\ln(2)}{c\varepsilon_0\pi r^2}P \tag{4}$$

where r is the approximate radius of the incident laser beam and P is the modulated laser power. The theoretical result based on Eq. (2) is demonstrated in Fig. 6(b), which is in good agreement with the experimental result for the TiS_2 nanosheet without the lines.

For the samples with the wire-grid-like structure, the THz transmittance descends clearly in comparison with that without the lines. Moreover, it seems to be very sensitive to the line

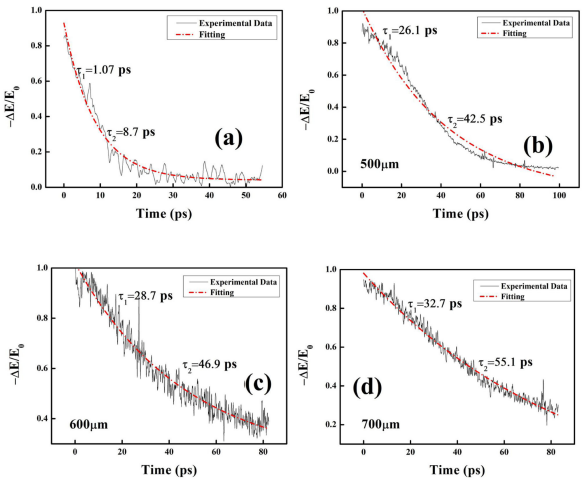

Fig. 7. Optical pump induced relative THz transmission change ($\Delta E/E0$) as a function of pump delay for TiS_2 nanofilms (a) without lines and lines with spacing (b) 500 μm, (c) 600 μm, and (d) 700 μm.

spacing. The larger the interval is, the faster the transmittance decreases under the same irradiation laser power. Therefore, the TiS_2 nanosheet devices that integrate the natural and structural properties should be more suitable as THz modulators.

B. OPTP Measurements of the TiS_2 Nanosheet Devices

In order to gain insight into the role of the sample structure further, the OPTP system was employed to investigate the conductivity response of the TiS_2 nanosheet and the devices. The initial terahertz peak field E_0 induced the peak field change ΔE of the transmitted THz wave. The relative change of $\Delta E/E_0$ as a function of probe time delay was recorded, as shown in Fig. 7. The measurements on the fabricated TiS_2 devices were done for several times to produce rather consistent and valid results.

Firstly, the time-resolved photoconductivity of the TiS_2 nanosheet is displayed in Fig. 7(a) The probe trace exhibits a fast rise in the photoconductivity and is followed by a biexponential decay. The maximum relative change of $\Delta E/E_0$ could be reached in a few picoseconds after the sample was resonantly excited by the femtosecond laser pulses, due to the fact that an absorbed photon could generate a hot electron-hole pair ion close to the band edge of the TiS_2, resulting in the maximum carrier density occurring within this time scale at a excitation pulse energy of 4.29 nJ. Subsequently, the hot carriers would decay through intraband thermal equilibrium and interband recombination.

The two relaxation processes could be fitted by a biexponential decay function containing a fast component τ_1 and a slow component τ_2, as Eq. (5) [12]:

$$-\frac{\Delta E}{E_0} = A_1 \exp\left(-\frac{\tau}{t_1}\right) + A_2 \exp\left(-\frac{\tau}{t_2}\right) \tag{5}$$

The relaxation processes of the biexponential decay can be interpreted as the carrier-carrier scattering and the carrier-phonon scattering, i.e., the fast decay τ_1 and the slow decay τ_2, respectively. The fitted curves are in good agreement with the experimental results.

For the TiS_2 nanofilm without the lines, $\tau_1 = 1.07\pm0.07$ ps and $\tau_2 = 8.7\pm0.13$ ps, as can be seen in Fig. 7(a). In comparison

TABLE I
TIME CONSTANTS OF CARRIER DYNAMICS OF TiS_2 AND SOME OTHER TRANSITION METAL DISULFIDE (TMD) MATERIALS

Materials	Band gap (eV)	Photoexcitation photon energy (eV)	τ_1 (ps)	τ_2 (ps)
Graphene [30]	0	1.55	-	2.79
MoS_2 [13]	1.2	2.53	0.66±0.15	-
WS_2 [32]	2	3.1	1~2	22
WS_2 [12]	1.93	3.1	0.6±0.1	5.4±0.2
WS_2 [12]	1.93	2.33	0.7±0.1	6±0.2
WSe_2 [14]	1.65	3.1	1	15
SnS_2 [15]	2.17	3.1	-	12±0.7
TiS_2 [this work]	Near 0[3]	1.19	1.07±0.07	8.7±0.13

with some other TMDs, the time constants of the reported carrier dynamics are summarized in Table I. The relaxation time extracted from the TiS_2 nanosheet is in reasonable agreement with those literature values, which illustrates that the data of the TiS_2 are comparable and reliable.

Afterwards, the TiS_2 devices with the lines were measured by the OPTP. The initial photoexcited carrier process in the devices and the TiS_2 nanosheet is the same. However, the exciting dynamics were found to be remarkably different from the one without the lines. τ_1 of the devices with the line spacings of 500 μm, 600 μm and 700 μm, are 26.1±0.1 ps, 28.7±0.13 ps and 32.7±0.15 ps, while τ_2 of the same samples are 42.5±0.2 ps, 46.9±0.22 ps and 55.1±0.26 ps, represented in Fig. 7(b), (c) and (d), respectively. Both the time constants of the relaxation processes are enlarged 27 and 5.5-fold in the devices than those in the TiS_2 nanosheet without the lines. The comparing experiments could demonstrate that the TiS_2 devices exhibited a rather long relaxation processes, which should be attributed to the fabricated structure on the devices. It has been recognized that the transient photoconductivity could be distinctly impacted by the size [33], morphoses [34], assembled structure [35] and molecular structure [36] of the semiconductor materials using the OPTP method, since the photoexcited carriers could be trapped onto these defect states and reduce the recombination velocity of the photoexcited carriers. For our TiS_2 devices, the isotopic property was broken by the lines, resulting in a combination structure of the wide bars of the TiS_2 nanosheet. As a consequence, the anisotropy of the diffusion range could make an impact on the average mobility due to the strong carrier localization on the surface boundaries arising from the surface depletion layer around these lines. Therefore, the mobility in these devices was slowed down and the decay time was delayed, as compared to those in the nanofilm without the lines. In addition, the increase of the line spacing was equivalent to a reduction of the surface defect states and would reduce the recombination velocity of the photoexcited carriers.

C. Photo-Induced Complex Conductivity Changes of TiS_2 Nanosheet

An alternative is to extract the time-dependent conductivity $\Delta\sigma(tp)$ from the measured $\Delta E(t,t_1)/E_0(t)$ data by varying the optical pump-THz probe delay (tp), which gives some insight into the physical mechanism behind this process. Here, $E(t,t_1)$

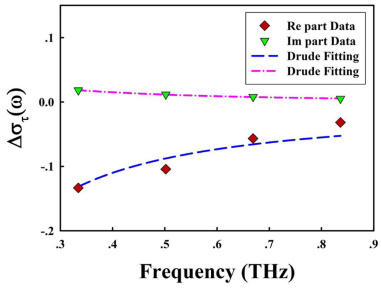

Fig. 8. Photo-induced complex conductivity change of TiS_2 nanofilm.

and $E_0(t)$ indicate the THz electric-field strengthes through the optical excited and unexcited TiS_2 devices, respectively, and $\Delta E(t,t_1) = E(t,t_1) - E_0(t)$. The transient photoconductivity variation $\Delta\sigma(tp)$ could be obtained by the relative transmission variation as [37]:

$$\Delta\sigma(t_1) = -\frac{1+n_s}{Z_0}\frac{\Delta E(t,t_1)}{E_0(t)} \tag{6}$$

where n_s and Z_0 represent the THz refractive index of the sapphire substrate and the impedance of free space, respectively. The excitation wavelength was 1040 nm (1.19 eV), whose photon energy is larger than the bandgap of the TiS_2 nanofilm (0.12∼0.24 eV).

The amplitude of the real part of the $\Delta\sigma(\tau, \omega)$ spectrum was reduced and the imaginary part of the $\Delta\sigma(\tau, \omega)$ spectrum was increased with increasing THz frequency. Our calculations and experimental results are consistent with the trend in [37]. We have modeled the transient response assuming the response of photo excitation, which can be explained the complex conductivity by the Drude-Smith model [38], [39]:

$$\sigma_{DS}(\omega) = \frac{\varepsilon_0 {\omega_p}^2 \tau}{1-i\omega\tau}\left(1+\frac{c}{1-i\omega\tau}\right) \tag{7}$$

where c accounts for the extent of carrier localization and back scattering in the thin film, ω_p is the plasma frequency, and τ is the Drude–Smith scattering time.

Then we fitted the pump-induced differential variation of the THz conductivity $\Delta\sigma(\tau, \omega)$ with ω_p and τ as adjustable parameters. The fitting results are given in Fig. 8 as the dashed lines, which show a good result in the frequency domain. A plasma frequency ω_p of 0.0078 THz and a Drude–Smith scattering time τ of 54.7 fs are obtained. In addition, the increasing layers of the 2D materials will lead to a higher photoconductivity [14], [40].

V. Conclusion

In conclusion, TiS_2 nanosheet-based devices have been ablated by a femtosecond laser. The modulation depth and the time-resolved photoconductivity of the TiS_2 devices with different line spacings were measured by THz-TDS and OPTP spectroscopy The experiments have demonstrated that the fabricated structure on the TiS_2 nanosheet contributed to the change of the optical-induced MD and the photoconductivity. The bi-exponential decay times were 1.07±0.07 ps and 8.7±0.13 ps for the TiS_2 nanosheet, and were 26.1±0.1 ps and 42.5±0.2 ps, 28.7±0.13 ps and 46.9±0.22 ps, and 32.7±0.15 ps and 55.1±0.26 ps for the devices with line spacings of 500 μm, 600 μm, and 700 μm, respectively. For the 700 μm ling spacing device, the optical-induced MD could reach 70%. A plasma frequency of 0.0078 THz and a Drude-Smith scattering time of 54.7 fs were also obtained. Our work provides insight into the ultrafast dynamics of THz photoconductivity in TiS_2 nanosheet devices and its good optical modulation performance.

References

[1] Y. Ge *et al.*, "Broadband nonlinear photoresponse of 2D TiS_2 for ultrashort pulse generation and all-optical thresholding devices," *Adv. Opt. Mater.*, vol. 6, no. 4, Dec. 2018, Art. no. 1701166.

[2] C. Lin *et al.*, "Hydrogen-incorporated TiS_2 ultrathin nanosheets with ultrahigh conductivity for stamp-transferrable electrodes," *J. Amer. Chem. Soc.*, vol. 135, no. 13, pp. 5144–5151, Mar. 2013.

[3] Z. Zhu *et al.*, "Near-infrared plasmonic 2D semimetals for applications in communication and biology," *Adv. Functional Mater.*, vol. 26, no. 11, pp. 1793–1802, Jan. 2016.

[4] C. M. Fang, R. A. D. Groot, and C. Haas, "Bulk and surface electronic structure of 1T–TiS_2 and 1T−$TiSe_2$," *Phys. Rev. B*, vol. 56, no. 8, Aug. 1997, Art. no. 4455.

[5] F. Rossi and T. Kuhn, "Theory of ultrafast phenomena in photoexcited semiconductors," *Rev. Modern Phys.*, vol. 74, no. 3, Aug. 2002, Art. no. 895.

[6] M. Rahm, J. S. Li, and W. J. Padilla, "THz wave modulators: A brief review on different modulation techniques," *J. Infrared, Milli., Terahz. Waves*, vol. 34, no. 1, pp. 1–27, Nov. 2013.

[7] T. Nozokido, H. Minamide, and K. Mizuno, "Modulation of submillimeter wave radiation by laser-produced free carriers in semiconductors," *Electron. Commun. Japan*, vol. 80, no. 6, pp. 1–9, Dec. 1997.

[8] I. H. Libon *et al.*, "An optically controllable terahertz filter," *Appl. Phys. Lett.*, vol. 76, no. 20, pp. 2821–2823, May 2000.

[9] E. Hendry *et al.*, "Ultrafast optical switching of the THz transmission through metallic subwavelength hole arrays," *Phys. Rev. B*, vol. 75, no. 23, Jun. 2007, Art. no. 235305.

[10] Z. H. Zhai *et al.*, "Enhanced photoresponses of an optically driven VO_2-based terahertz wave modulator near percolation threshold," *Appl. Phys. Lett.*, vol. 113, no. 23, Dec. 2018, Art. no. 231104.

[11] F. Hu *et al.*, "Photo-induced high modulation depth terahertz modulator based on VOx–Si–VOx hybrid structure," *J. Phys. D Appl. Phys.*, vol. 52, no. 17, Apr. 2019, Art. no. 175103.

[12] S. Xu *et al.*, "Transient photoconductivity and free carrier dynamics in a monolayer WS_2 probed by time resolved terahertz spectroscopy," *Nanotechnology*, vol. 30, no. 26, Mar. 2019, Art. no. 265706.

[13] P. D. Cunningham *et al.*, "Charge trapping and exciton dynamics in large-area CVD grown MoS_2," *J. Phys. Chem. C*, vol. 120, no. 10, pp. 5819–5826, Feb. 2016.

[14] C. J. Docherty *et al.*, "Ultrafast transient terahertz conductivity of monolayer MoS_2 and WSe_2 grown by chemical vapor deposition," *ACS Nano*, vol. 8, no. 11, pp. 11147–11153, Oct. 2014.

[15] W. Zhang *et al.*, "Probing the charge carrier dynamics and photoconductivity of few-layer SnS_2 by optical pump-THz probe spectroscopy," in *Proc. Int. Symp. Ultrafast Phenomena Terahertz Waves*, Changsha, China, 2018, Paper TuK9.

[16] S. J. Varma *et al.*, "2D TiS_2 layers: A superior nonlinear optical limiting material," *Adv. Opt. Mater.*, vol. 5, no. 24, Oct. 2017, Art. no. 1700713.

[17] J. H. Shi *et al.*, "THz photonics in two dimensional materials and metamaterials: Properties, devices and prospects," *J. Mater. Chem. C*, vol. 6, no. 6, pp. 1291–1306, Feb. 2018.

[18] J. L. Zheng *et al.*, "Few-layer phosphorene-decorated microfiber for all-optical thresholding and optical modulation," *Adv. Opt. Mater.*, vol. 5, no. 9, May 2017, Art. no. 1700026.

[19] L Lu *et al.*, "All-optical switching of two continuous waves in few layer bismuthene based on spatial cross-phase modulation," *ACS Photon.*, vol. 4, no. 11, pp. 2852–2861, Nov. 2017.

[20] Y. Z. Wang *et al.*, "All-optical phosphorene phase modulator with enhanced stability under ambient conditions," *Laser Photon. Rev.*, vol. 12, no. 6, Jun. 2018, Art. no. 1800016.

[21] P. Gopalan *et al.*, "2D materials for terahertz modulation," *Adv. Opt. Mater.*, vol. 8, no. 3, Aug. 2019, Art. no. 1900550.

[22] Y. Li *et al.*, "Polarization modulation of terahertz wave by femtosecond laser additive manufactured tin grating," *Infrared Phys. Technol.*, vol. 95, pp. 76–80, Dec. 2018.

[23] D. Palima *et al.*, "Diffractive generalized phase contrast for adaptive phase imaging and optical security," *Opt. Express*, vol. 20, no. 2, pp. 1370–1377, Jan. 2012.

[24] G. A. Mourou *et al.*, "Optics in the relativistic regime," *Rev. Modern Phys.*, vol. 78, no. 2, pp. 309–371, Apr./Jun. 2006.

[25] P. C. Sherrell *et al.*, "Thickness-dependent characterization of chemically exfoliated TiS_2 nanosheets," *ACS Omega*, vol. 3, pp. 8655–8662, Aug. 2018.

[26] P. C. Klipstein *et al.*, "Stoichiometry dependence of the transport properties of TiS_2," *J. Phys. C Solid State Phys.*, vol. 14, no. 10, Oct. 1981, Art. no. 4067.

[27] S. J. Sandoval *et al.*, "Raman spectra of Ag_xTiS_2 and lattice dynamics of TiS_2," *Phys. Rev. B*, vol. 45, no. 24, Jun. 1992, Art. no. 14374.

[28] J. Shi *et al.*, "Femtosecond pulse coupling dynamics between a dispersion-managed soliton oscillator and a nonlinear amplifier in an all-PCF-based laser system," *Optik*, vol. 145, pp. 569–575, Sep. 2017.

[29] Y. S. Ang, S. Sultan, and C. Zhang, "Nonlinear optical spectrum of bilayer graphene in the terahertz regime," *Appl. Phys. Lett.*, vol. 97, no. 24, Dec. 2010, Art. no. 243110.

[30] D. S. Yang, T. Jiang, and X. A. Cheng, "Optically controlled terahertz modulator by liquid-exfoliated multilayer WS_2 nanosheets," *Opt. Express*, vol. 25, no. 14, pp. 16364–16377, Jul. 2017.

[31] Q. Y. Wen *et al.*, "Graphene based all-optical spatial terahertz modulator," *Sci. Rep.-UK*, vol. 4, Dec. 2014, Art. no. 7409.

[32] X. Xing *et al.*, "Role of photoinduced exciton in the transient terahertz conductivity of few-layer WS_2 laminate," *J. Phys. Chem. C*, vol. 121, no. 37, pp. 20451–20457, Aug. 2017.

[33] M. J. Li *et al.*, "Size and surface effects on transient photoconductivity in CdS nanobelts probed by time-resolved terahertz spectroscopy," *Appl. Phys. Lett.*, vol. 101, no. 9, Aug. 2012, Art. no. 091104.

[34] J. Lloyd-Hughes *et al.*, "Influence of surface passivation on ultrafast carrier dynamics and terahertz radiation generation in GaAs," *Appl. Phys. Lett.*, vol. 89, no. 23, Dec. 2006, Art. no. 232102.

[35] R. P. Prasankumar *et al.*, "Carrier dynamics in self-assembled ErAs nanoislands embedded in GaAs measured by optical-pump terahertz-probe spectroscopy," *Appl. Phys. Lett.*, vol. 86, no. 20, May 2005, Art. no. 201107.

[36] O. Ostroverkhova *et al.*, "Anisotropy of transient photoconductivity in functionalized pentacene single crystals," *Appl. Phys. Lett.*, vol. 89, no. 19, Nov. 2006, Art. no. 192113.

[37] G. Jnawali *et al.*, "Observation of a transient decrease in terahertz conductivity of single-layer graphene induced by ultrafast optical excitation," *Nano Lett.*, vol. 13, no. 2, pp. 524–530, Jan. 2013.

[38] R. Ulbricht *et al.*, "Carrier dynamics in semiconductors studied with time-resolved terahertz spectroscopy," *Rev. Modern Phys.*, vol. 83, no. 2, Jun. 2011, Art. no. 543.

[39] D. G. Cooke *et al.*, "Transient terahertz conductivity in photoexcited silicon nanocrystal films," *Phys. Rev. B*, vol. 73, no. 19, May 2006, Art. no. 193311.

[40] S. Sim *et al.*, "Ultrafast terahertz dynamics of hot Dirac-electron surface scattering in the topological insulator Bi_2Se_3," *Phys. Rev. B*, vol. 89, no. 16, Apr. 2014, Art. no. 165137.

Qi Song is now a doctorate degree candidate at Ultrafast Laser Laboratory, Tianjin University. His research interests focus on the 2D materials in lasers and THz applications.

Lu Chai received the Ph.D. degree in optical engineering from Tianjin University, China, in 1998. In 1994, he joined the Ultrafast Laser Laboratory, School of Precision Instruments and Optoelectronics Engineering, Tianjin University. He was a Visiting Scholar with The Hong Kong University of Science and Technology from 1995 to 1997. He is currently a professor. His research interests focus on the generation and characterization of ultrashort THz emitters, modulators and their applications.

Junqi Chen received the B.S. degree in electronic engineering from Tianjin University in 2017. He is now a master degree candidate at Ultrafast Laser Laboratory, Tianjin University. His research interests include modulators for terahertz waves.

Weining Liu received the B.S. degree in electronic engineering from Tianjin University in 2017, where he is currently pursuing his M.S. degree in optical engineering. His research interests include 2D material-based nanosheets and modulatiors for terahertz waves.

Qing Ma received the B.S. degree in electronic engineering in 2017 from Tianjin University, where he is currently pursuing the M.S. degree in optical engineering. His research interests include terahertz wave generation.

Yanfeng Li received the B.S. degree in optoelectronics and the Ph.D. degree in optical engineering from Tianjin University, Tianjin, China, in 1999 and 2005, respectively. He first worked as a Postdoctoral Fellow at Tianjin University, where he has been an Associate Professor with Ultrafast Laser Laboratory ever since. His current research interests include terahertz photonics and terahertz plasmonic and metamaterial devices. Prof. Li is a member of the Optical Society of America.

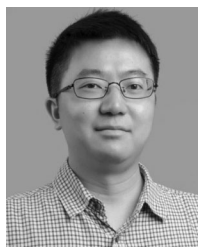

Minglie Hu received the B.Sc. degree in electrical engineering from the School of Precision Instruments and Optoelectronics Engineering, and the Ph.D. degree in optical engineering from Tianjin University in 2000 and 2005, respectively. He is currently a Professor at School of Precision Instruments and Optoelectronics Engineering, Tianjin University. His current research interests include mode-locking laser oscillators and amplifiers, fiber lasers, nonlinear and linear propagation in photonic crystal fibers, and THz photonics.